Finite element analyses for predicting anatomical neck fractures in the proximal humerus

Gal Dahan[a], Nir Trabelsi[b], Ori Safran[c], Zohar Yosibash[a]

[a]*School of Mechanical Engineering, The Iby and Aladar Fleischman Faculty of Engineering, Tel-Aviv University, Ramat-Aviv, Israel - yosibash@tauex.tau.ac.il*
[b]*Department of Mechanical Engineering, Shamoon College of Engineering, Beer-Sheva, Israel*
[c]*Department of Orthopaedics, Hadassah University Hospital, Jerusalem, Israel*

Abstract

Background: Proximal humerus fractures which occur as a result of a fall on an outstretched arm are frequent among the elderly population. The necessity of stabilizing such fractures by surgical procedures is a controversial matter among surgeons. Validating a personalized FE analysis by ex-vivo experiments of humeri and mimicking such fractures by experiments is the first step along the path to determine the necessity of such surgeries.

Methods: Four fresh frozen human humeri were loaded using a new simple experimental setting, so to fracture the humeri at the anatomical neck. Strains on humeri's surfaces predicted by the high order FE analyses (as in [9]) were compared to the experimental observations to further enhance the validity of the FE analyses. A simplified yield criterion based on a linear elastic analysis and principal strains was used to predict the anatomical neck fracture as observed in the experiment.

Findings: An excellent correlation between experimental measured and FE predicted strains was obtained (slope of 0.99 and R^2 =0.98). All humeri were fractured at the anatomical neck. The predicted yield load was within 10%-20% accuracy.

Interpretation: High-order FE analyses reliably predict strains and yield loads in the humeri. Fractures induced by the experimental setting correspond to anatomical neck fractures noticed in practice and classified as AO C1.1-C1.3. Surgical neck fractures, which are most common in clinical practice, could not be realized in the proposed experiments, and a different experimental setting should be sought to obtain them ex-vivo.

Keywords: Humerus, FEMs, anatomic neck fracture

1. Introduction

Proximal humerus fractures as a result of a fall on an outstretched arm are usually classified as displaced or minimally to non-displaced, based on the distance between fracture's fragments. Minimally and non-displaced fractures are mostly treated conservatively [26, 3], and the necessity of a fixation surgery for such fractures remains controversial. Agreement on the treatment and even identification of fractured fragments is reported as limited [6, 26, 12, 7]. An important factor in deciding on the need for surgical intervention is the stability of fracture, i.e. the likelihood that fractured fragments would move during rehabilitation and minor arm movements. A patient specific finite element analysis (FEA), based on quantitative computed tomography (QCT) scans, may be used to determine bone residual strength following fracture, thus enabling assessing fracture's stability. With the high incidence of proximal humerus fractures in the elderly [8, 19, 4], and the growing incidence of surgically treated fractures and revision surgeries [3], there is a growing need for such a biomechanical-based quantitative tool. As a first step towards such FEAs of proximal humeri, we aim at developing and experimentally validating a verified FE model to reliably predict the mechanical response of the intact proximal humerus up to fracture.

In a previous work [9], we introduced both mechanical testing and an ex-vivo fracture experiments of four fresh frozen proximal humeri. FEAs of humeri were successfully validated based on two of the four experiments because the experimental boundary conditions on the other two were not possible to be identified in the FEA. Furthermore,the experimental setting that induced fractures in the four humeri could not have been simulated by the FEAs. Here, we enhance our previous work by: (a) Enhancing the experimental database by four additional humeri on which physiological-like loads are applied, (b) Introducing a new experimental device that allows to induce impacted fractures at the anatomical neck, while applying well-defined boundary conditions that can be well represented in the FE simulations, and (c) Validating a yield criterion that can be used to predict yield load in the proximal humeri.

Several past studies have addressed fractures of the proximal humerus, however the focus of these are osteotomies, studying different fixations both experimentally and by FE models [20, 31, 32]. We hypothesize that a simple ex-vivo experimental configuration can be used to induce anatomic neck fracture in proximal humeri, and the yield load and fracture initiation location may be predicted by FEA using the simplified yield criterion described in [35].

2. Methods

Four human humeri (2 pairs, denoted by FFH3 and FFH4, obtained from the National Disease Research Interchange, Philadelphia, PA, USA), were experimentally tested. Donors' details are:

Donor Label	Age (Years)	Height [m]	Weight [Kg]	Gender
FFH3	72	1.63	41	Female
FFH4	67	1.78	84	Male

Experiments were conducted on each pair (right and left) on the same day of defrosting. Prior to mechanical testing, the humeri were cleaned of soft tissue, cut, mounted into a steel cylinder and CT scanned while immersed in water with five K_2HPO_4 calibration solutions (concentrations: 0,50,100,200 and 300 mg/cc, prepared according to [21]). Humeri were scanned using a Brilliance 64 scanner (Philips Healthcare, Eindhoven, The Netherlands). The scanning parameters were 120 kVp, slice thickness of 1.25 mm (equal to slice spacing), exposure of 250 mAs and pixel sizes of 0.195, 0.177, 0.237 and 0.209 mm for FFH3 L & R and FFH4 L & R respectively. Detailed specimen preparation procedures are given in [9].

2.1. Experimental methods

2.1.1. Elastic Response

The humeri were loaded at three configurations, two that simulate physiological-like loadings, based on angles ranges reported in [5], and one that simulates a fall on an out-stretched arm (Figure 1 right). Loads directions are defined using two angles- α and β, in a coordinate system on the right proximal humerus suggested by [33]: System origin is located in the center

of the humeral head (glenohumeral rotation center), y axis is the line connecting the origin and the midpoint between the lateral and the medial epicondyles, pointing upwards; x axis is perpendicular to the plane formed by the origin and the two epicondyles, pointing forward; and z axis is the line vertical to the xy plane, pointing right. α and β are the angles of the loading vector projection on yz and xy planes respectively (see Figure 1 left). For simulating physiological-like loads, the bones were fixed to two jigs cut at different inclinations in the yz and xy planes, resulting in $\alpha = 26.4°$ and $\beta = 20°$ and $\alpha = 36°$ and $\beta = 16.6°$. These angles are within the range measured by [5] who studied the loads applied on the humeral head during simple arm movements. To simulate a fall on an out-stretched arm, the humeri were rotated at 25° about the y axis to align in the scapular plane (The anatomical plane of the scapula bone in the body, in which the center of the humeral head is aligned), and then fixed to the testing machine at a 20° angle while facing downwards, their head connected to a PMMA base (20mm diameter) using a screw. This fixation assured a contact area which is constant both in size and location, and assured a fracture in the proximal part of the bone rather than in the distal part. (resulted angles in bone's system: $\alpha = 18.3°$ and $\beta = 8.7°$). One of the humeri- FFH3R, was fixed to the load cell at 0° rather than 20° ($\alpha = \beta = 0°$). Displacement controlled loadings (resulting in 300-700 N in the vertical direction) were applied. 3 forces and 3 moments were measured using a 6-axis load cell (ATI Omega 191). Strains were recorded using 11-14 uniaxial strain gauges (SGs) (Vishay C2A-06-125LW-350, $\pm 0.2\%$ precision) bonded to the bones' surface. Linear correlation between measured strains and force was verified, and the resulting strain for a 800 N load was computed. Locations of the SGs on the humeri are shown in Figure 2. All recorded strains during the experiment are summarized in the supplementary material.

[Figure 1 about here.]

[Figure 2 about here.]

2.1.2. Proximal humerus fractures

Following experiments in the elastic regime, each humerus was loaded up to fracture with load applied according to third configuration described in section 2.1.1. A displacement was

applied to the humeri until fracture, observed at $\sim$ 8 mm. Experimental yield load was defined as the maximum recorded force before deviation from linearity at the force-strain curve of the closest SG to fracture. To determine the point of deviation, a linear trendline was fit to the curve and the intersection of the force-strain response with a 5 % deviation of the this trendline slope was defined as the yield point, as suggested in [35].

2.2. FEA

High order finite element (p-FE) linear elastic analyses mimicking the experimental loadings were performed. These QCT-based p-FE models were semi-automatically constructed using an in-house Matlab code. A computer-aided design (CAD) model was generated using Solidworks (Dassault Systèmes, Waltham, MA, USA), and thereafter imported to Stress-Check (ESRD, St. Louis, MO, USA), a p-FE software. Models were auto-meshed using high-order tetrahedral elements ($2700 - 3900$ elements, resulting in 0.7-1 million DOF at $p = 8$). HU values from the scan were used to determine the material properties. To account for noise and boundary effects present in the CT images, the HU values were first corrected at the boundary and smoothed using a moving average algorithm (details are available in [16]). Using the calibration solutions scanned with the bones, a linear relation was set to relate each voxel's HU value to the equivalent mineral density of the solution ($\rho_{K_2HPO_4}$). This density was then converted to ash density (ρ_{ash}) using a relation between hydroxyapatite and K_2HPO_4 solutions (as suggested by [13], Eq. 1) and a conversion proposed by [27] (Eq. 2)

$$\rho_{hydroxyapatite}\ [gr/cm^3] = 1.15 \times \rho_{K_2HPO_4} \tag{1}$$

$$\rho_{ash}\ [gr/cm^3] = 0.877 \times \rho_{hydroxyapatite} + 0.08 \tag{2}$$

Finally, Young's modulus was calculated from ρ_{ash} based on [18] and [17] (Eq. 3), as in [34, 9]:

$$
\begin{aligned}
E_{cort} &= 10200 \cdot \rho_{ash}^{2.01}\ [MPa], \qquad \rho_{ash} > 0.486\ [gr/cm^3] \\
E_{trab} &= 2398\ [MPa], \qquad 0.3 < \rho_{ash} \leq 0.486\ [gr/cm^3] \\
E_{trab} &= 33900 \cdot \rho_{ash}^{2.2}\ [MPa], \qquad \rho_{ash} \leq 0.3\ [gr/cm^3]
\end{aligned} \tag{3}
$$

E_{cort} and E_{trab} are Young's moduli for cortical and trabecular bone respectively. Poisson's ratio was set to 0.3. Inhomogeneous material properties were assigned to each integration point, based on the closest voxel found in the CT scan, thus having a varying Young's modulus within each element (512 values for each element).

Models were fixed at the bones' distal face ($\vec{u} = 0$) and a load was applied to the humeral head (F_z=800 N and F_x,F_y according to the measured forces in the experiment). The p-FE models were solved by increasing the polynomial degree to obtain convergence in energy norm. Local convergence in principal strains was verified at SGs locations, FE strains were averaged along 3 mm lines corresponding to SG active gauge length. For the model that simulated the loading to induce a fracture, u_x=u_y=0 was verified at the humeral head, as it was fixed in the experiments.

The FE yield load prediction was computed using a maximum principal strain criterion [28, 35]. Since the bone is known to have a linear response up to the yield point, a simple linear extrapolation was used to calculate the load at which a critical strain value is obtained. Yielding was assumed to occur in the trabecular tissue inside the humeral head because of the very thin layer of cortex that cannot act as a shielding structure in the neck and head regions, and only then to propagate to the outer cortical surface. To obtain a broad understanding of the yield prediction and to test this assumption, yield loads were computed for both the trabecular region inside humerus head and neck and the cortical layer. The yield load was the one that induces maximum compression strain in the FEA that equals the compression yield strain proposed by [2] and [15] (for trabecular and cortical bone respectively):

$$\varepsilon_{y-trab} = \quad -10400\ [\mu strain] \tag{4}$$
$$\varepsilon_{y-cort} = \quad -8600\ [\mu strain]$$

The locations of the predicted maximum strain were also compared to the experiments.

2.3. Statistical Analysis of the Results

Agreement between experimental and FE strains was determined by linear correlation (LC) and Bland-Altman (BA) [1] plots. In addition to the simple linear regression (common simplified statistical analysis in studies similar to the presented one), we conducted a linear mixed model (LMM) analysis. The LMM accounts for data points not being all independent, such as multiple SGs on same specimen and three strain measurements by each SG due to three different loadings. Specific SG and loading configuration were defined as factors having a random effect in the model (both nested in the bone factor). The linear slope and intercept from both statistical methods was compared. Both methods assume normality and homoscedasticity of the model residuals, therefore these assumptions were examined. The mean absolute percentage error and the root mean square error (RMSE) are also reported, along with the mean absolute strain:

$$\text{Mean absolute relative error } = \frac{100}{N} \sum_{i=1}^{N} \left| \frac{\left(\varepsilon_{Exp(i)} - \varepsilon_{FE(i)}\right)}{\varepsilon_{Exp(i)}} \right| \ \ [\%] \tag{5}$$

$$\text{RMSE } = \sqrt{\frac{1}{N} \sum_{i=1}^{N} \left(\varepsilon_{Exp(i)} - \varepsilon_{FE(i)}\right)^2} \ \ [\mu strain] \tag{6}$$

$$\text{Mean absolute strain } = \frac{1}{N} \sum_{i=1}^{N} \left| \frac{\left(\varepsilon_{Exp(i)} + \varepsilon_{FE(i)}\right)}{2} \right| \ \ [\mu strain] \tag{7}$$

N is the total number of SG data from different loading conditions. For a comprehensive overview of all results obtained so far, we also present the FE-Exp correlation obtained for all 6 experiments (included FFH2 from previous study [9]).

For the yield load, agreement was analyzed in terms of percentage difference and also by observing fracture location in the experiment versus the location where the maximum absolute strain was obtained in the FE model.

3. Results

A linear response between force and strain was observed at all SGs in the experiments in the elastic range . All FE models converged to less than 7% error in energy norm at $p = 8$. Forces vs. strain at the SG closest to the fracture location for the four humeri (experiments leading to fracture) are shown in Fig. 3.

[Figure 3 about here.]

LC and BA plots of strains measured on the four humeri at the three loading configurations, and the twelve FE analyses are presented in Fig. 4. The fixed slope and intercept obtained from the LMM were almost similar to these obtained in the simple linear regression (slope and intercept of 0.976 and -26 compared to 0.998 and -63). Normal distribution and homoscedasticity of the residuals was confirmed. The mean absolute strain, mean absolute relative error and RMSE are summarized in Table 1. The full experimental data and FE results are provided in the Supplementary Material.

[Figure 4 about here.]

[Table 1 about here.]

Fracture locations from experiments vs. location of FE maximum compression strain (ε_3) in the trabecular and cortical areas are presented in Fig. 5. Relevant loads are summarized in Table 2.

[Figure 5 about here.]

[Table 2 about here.]

For a full analysis of all experiments and models conducted so far, Fig. 6 presents LC and BA plots of data pooled from all 6 humeri (FFH3 and FFH4 from this paper and FFH2 from [9]).

[Figure 6 about here.]

4. Discussion

This study is an expanded and enhanced investigation following the work presented in [9]. Four additional humeri were tested, a new jig to induce anatomic neck fractures was constructed and used for testing and new FEAs were performed. The four new samples of the current study show an excellent correlation between experiments and FEA predicted strains (Fig. 4-left):

$$FE = 0.998 \times EXP - 63.4 \ , \ \ R^2 = 0.983. \tag{8}$$

FE and EXP refer to the model predicted strains and the experimentally measured strains respectively. The correlation obtained using LMM (fixed slope and intercept) was almost identical to the one obtained using a simple linear regression, suggesting that the latter is sufficient for the analysis of the results. The excellent correlation between FE and EXP strengthen our confidence in the FE analysis that has already been validated in our previous study on two humeri only (slope of 1.09 and $R^2 = 0.982$). The Bland-Altman plot for the four new humeri (Fig. 4 right) shows no bias between FE and EXP strains. Inspecting Table 1, one notices a slightly better agreement in the shaft region compared to the neck, when inspecting both mean absolute error and RMSE (compared to mean absolute strain). This can be due to the misrepresentation of the neck region by isotropic material properties.

Four humeri were fractured in [9], using an experimental jig that did not allow a proper determination of the boundary conditions in the FEA, thus a comparison of the predicted

vs. measured yield load could not be obtained. The new experimental jig in this study allowed to perform fracture experiments on four additional humeri, for which the boundary conditions could had been properly represented in the FEA. Figure 5 demonstrated that fracture initiation location was properly predicted by the FEA for all four humeri. As for the yield loads, they were predicted with an accuracy of 10%-20% when using the cortex yield criterion and conservative predictions were obtained, i.e. predicted yield load was smaller compared to experimental values (Table 2).

Combining all data from 6 humeri from both studies (Fig. 6-left), the following correlation is obtained:

$$FE = 1.03 \times EXP - 82.9 \ , \ \ R^2 = 0.982. \tag{9}$$

The BA plot of all 6 humeri (Fig. 6-right) shows a small negative bias (~ -80 μstrain) suggesting that overall the FE models predicts a response which is less-stiff than the experiments.

In clinical practice two classifications for proximal humeri fractures as seen in our experiments are used: Neer [23] and AO [22]. All 8 humeri tested by the authors fractured at the anatomical neck, some involved also a separation of the greater tuberosity (GT) with the head being at a slight varus (inward) or valgus (outward) malalignment. Using Neer classification, we found Neer type II fracture as the suitable classification for all 8 fractures. Although it describes an *isolated* anatomical neck fracture, all other fractures defined by Neer that include the anatomical neck are 3 and 4 part fractures thus they were inappropriate. The AO classification is a more detailed classification system, describing 27 different fractures, thus it was found to be more appropriate for classifying the fractures obtained in the experiments; the eight fractured humeri classified by AO and the X-ray scans of the relevant classification are illustrated in Figure 7 and summarized in Table 3.

[Table 3 about here.]

To the best of our knowledge, this is the first study to report physiological proximal humerus fractures generated by an experimental jig using fresh frozen humeri, and FEA prediction of these fractures. In [29], 7 different fracture types are mentioned, obtained by a single loading configuration, but no photos showing the resulted fractures are presented in the paper. In [10], proximal cadaver humeri were *bent* to create a fracture, no details on the experimental system are given, nor photos of the resulted fractures or their specific classification.

There are three limitations to this study, material properties representation, incidence of the obtained fractures and the small sample size. The humeri were modeled as isotropic, although bone is known to be orthotropic. Isotropic material properties were shown to be sufficient for simple loadings on the femur [36, 30], however for the proximal humeri this assumption and the influence of using orthotropic material properties in FE models should be evaluated. Fractures in the anatomical neck of the humerus are physiological but somewhat uncommon (up to 5%, as reported in [24, 11, 4, 25]). In a future study we aim to include ex-vivo experiments to obtain impacted fractures at the surgical neck of humeri, which are the more common fracture type in the proximal humerus (incidence of 20%-37% as reported in [14, 11, 4]). Finally, we validated the mechanical response on 6 humeri from three donors and the yield on 4 humeri from two donors. Further validation on more humeri would increase the credibility of FE methods as a tool to be used in clinical practice.

[Figure 7 about here.]

5. Conclusions

High-order FEA of humeri were validated by experiments on four fresh-frozen bones. Experiments on these humeri were conducted in various configurations to simulate physiological loadings and induce fractures at the anatomical neck. An excellent correlation was demonstrated between measured and predicted strains in the elastic regime. The humeri

were successfully fractured at the anatomical neck (AO C1.1-C1.3 fractures). The FE predicted yield loads estimated the experimental yield loads within a difference of less than 20% (conservative predictions). Future experiments designed to induce fractures at the surgical neck and their simulation by FE methods will enhance the validity of these methods towards their use in daily clinical practice.

Conflict of Interest

None of the authors have any conflict of interest to declare that could bias the presented work.

Acknowledgements

The authors thank Dr. Lena Novack from the Ben-Gurion University and Prof. Malka Gurfine from Tel-Aviv University for their assistance with the statistical study, and Mr. Ilan Gilad and Mr. Yekutiel Katz, from Tel Aviv University for their assistance with the experiments. This study was made possible through the generous support of Milgrom Foundation for Science grant.

References

[1] Altman, D.G., Bland, J.M., 1983. Measurement in medicine: The analysis of method comparison studies. Source Journal of the Royal Statistical Society 32, 307–317.

[2] Bayraktar, H.H., Morgan, E.F., Niebur, G.L., Morris, G.E., Wong, E.K., Keaveny, T.M., 2004. Comparison of the elastic and yield properties of human femoral trabecular and cortical bone tissue. Journal of Biomechanics 37, 27–35.

[3] Bell, J., Leung, B.C., Spratt, K.F., Koval, K.J., Weinstein, J.D., Goodman, D.C., Tosteson, A., 2011. Trends and Variation in Incidence, Surgical Treatment, and Repeat Surgery of Proximal Humeral Fractures in the Elderly. The Journal of Bone and Joint Surgery-American Volume 93, 121–131.

[4] Bergdahl, C., Ekholm, C., Wennergren, D., Nilsson, F., Möller, M., 2016. Epidemiology and patho-anatomical pattern of 2,011 humeral fractures: data from the Swedish Fracture Register. BMC Musculoskeletal Disorders 17, 159.

[5] Bergmann, G., Graichen, F., Bender, A., Rohlmann, A., Halder, A., Beier, A., Westerhoff, P., 2011. In vivo gleno-humeral joint loads during forward flexion and abduction. Journal of Biomechanics 44, 1543–52.

[6] Bernstein, J., Adler, L.M., Blank, J.E., Dalsey, R.M., Williams, G.R., Iannotti, J.P., 1996. Evaluation of the Neer system of classification of proximal humeral fractures with

computerized tomographic scans and plain radiographs. J Bone Joint Surg Am 78, 1371–1375.

[7] Bruinsma, W.E., Guitton, T.G., Warner, J.J.P., Ring, D., 2013. Interobserver reliability of classification and characterization of proximal humeral fractures. Journal of Bone and Joint Surgery - Series A 95, 1600–1604.

[8] Court-Brown, C.M., Garg, A., McQueen, M.M., 2001. The epidemiology of proximal humeral fractures. Acta Orthopaedica 72, 365–371.

[9] Dahan, G., Trabelsi, N., Safran, O., Yosibash, Z., 2016. Verified and validated finite element analyses of humeri. Journal of Biomechanics 49, 1094–1102.

[10] Fankhauser, F., Schippinger, G., Weber, K., H., H., Heinz, K., Quehenberger, F., Boldin, C., Bratschitsch, G., Szyszkowitz, R., Georg, L., Friedrich, A., 2003. Cadaveric-biomechanical evaluation of bone-implant construct of proximal humerus fractures (Neer type 3). The Journal of Trauma 55, 345–9.

[11] Fjalestad, T., Strømsøe, K., Blücher, J., Tennøe, B., 2005. Fractures in the proximal humerus: functional outcome and evaluation of 70 patients treated in hospital. Archives of Orthopaedic and Trauma Surgery 125, 310–316.

[12] Foroohar, A., Tosti, R., Richmond, J.M., Gaughan, J.P., Ilyas, A.M., 2011. Classification and treatment of proximal humerus fractures: inter-observer reliability and agreement across imaging modalities and experience. Journal of Orthopaedics Surgery and Research 6, 1–9.

[13] Goodsitt, M.M., 1992. Conversion relations for quantitative CT bone mineral densities measured with solid and liquid calibration standards. Bone and Mineral 19, 145–158.

[14] Hanson, B., Neidenbach, P., de Boer, P., Stengel, D., 2009. Functional outcomes after nonoperative management of fractures of the proximal humerus. Journal of Shoulder and Elbow Surgery 18, 612–21.

[15] Kaneko, T.S., Pejcic, M.R., Tehranzadeh, J., Keyak, J.H., 2003. Relationships between material properties and CT scan data of cortical bone with and without metastatic lesions. Medical Engineering and Physics 25, 445–454.

[16] Katz, Y., Dahan, G., Sosna, J., Shelef, I., Cherniavsky, E., Yosibash, Z., 2019. Scanner influence on the mechanical response of QCT-based finite element analysis of long bones. Journal of Biomechanics 86, 149–159.

[17] Keller, T.S., 1994. Predicting the compressive mechanical behavior of bone. Journal of Biomechanics 27, 1159–1168.

[18] Keyak, J., Kaneko, T.S., Tehranzadeh, J., Skinner, H., 1994. Correlations between orthogonal mechanical properties and density of trabecular bone: Use of different densitometric measures. Biomedical Materials 28, 1329–1336.

[19] Kim, S.H., Szabo, R.M., Marder, R.A., 2012. Epidemiology of humerus fractures in the United States: Nationwide emergency department sample, 2008. Arthritis Care and Research 64, 407–414.

[20] Maldonado, Z., Seebeck, J., Heller, M., Brandt, D.and Hepp, P., Lill, H., Duda, G., 2003. Straining of the intact and fractured proximal humerus under physiological-like loading. Journal of Biomechanics 36 36, 1865–1873.

[21] Mindways Software, I., 2002. Calibration Phantom Users Guide. Technical Report. Austin, TX, USA.

[22] Muller, M., Nazarian, S., Koch, P., Schatzker, J., 1990. The comprehensive classification of fractures of long bones. Springer-Verlag, Berlin.

[23] Neer, C., 1970. Displaced proximal humeral fractures. I. Classification and evaluation. J Bone Joint Surg Am 52, 1077–1089.

[24] Orozco, R., Sales, J., Videla, M., 2000. Atlas of Internal Fixation. Springer-Verlag, Berlin.

[25] Papakonstantinou, M.K., Hart, M.J., Farrugia, R., Gabbe, B.J., Kamali Moaveni, A., van Bavel, D., Page, R.S., Richardson, M.D., 2016. Interobserver agreement of Neer and AO classifications for proximal humeral fractures. ANZ Journal of Surgery 86, 280–284.

[26] Petit, C.J., Millett, P.J., Endres, N.K., Diller, D., Harris, M.B., Warner, J., 2010. Management of proximal humeral fractures: Surgeons don't agree. Journal of Shoulder and Elbow Surgery 19, 446–451.

[27] Schileo, E., Dall'Ara, E., Taddei, F., Malandrino, A., Schotkamp, T., Baleani, M., Viceconti, M., 2008a. An accurate estimation of bone density improves the accuracy of subject-specific finite element models. Journal of Biomechanics 41, 2483–2491.

[28] Schileo, E., Taddei, F., Cristofolini, L., Viceconti, M., 2008b. Subject-specific finite element models implementing a maximum principal strain criterion are able to estimate failure risk and fracture location on human femurs tested in vitro. Journal of Biomechanics 41, 356–367.

[29] Skedros, J.G., Knight, A.N., Pitts, T.C., O'Rourke, P.J., Burkhead, W.Z., 2016. Radiographic morphometry and densitometry predict strength of cadaveric proximal humeri more reliably than age and DXA scan density. Journal of Orthopaedic Research 34, 331–341.

[30] Trabelsi, N., Yosibash, Z., 2011. Patient-specific finite-element analyses of the proximal femur with orthotropic material properties validated by experiments. Journal of Biomechanical Engineering 133, 061001.

[31] Varga, P., Grünwald, L., Inzana, J.A., Windolf, M., 2017. Journal of the Mechanical Behavior of Biomedical Materials Fatigue failure of plated osteoporotic proximal humerus fractures is predicted by the strain around the proximal screws. Journal of the Mechanical Behavior of Biomedical Materials 75, 68–74.

[32] Varga, P., Inzana, J.A., Gueorguiev, B., Südkamp, N., Windolf, M., 2018. Validated

computational framework for efficient systematic evaluation of osteoporotic fracture fixation in the proximal humerus. Medical Engineering and Physics 57, 29–39.

[33] Wu, G., Van Der Helm, F.C., Veeger, H.E., Makhsous, M., Van Roy, P., Anglin, C., Nagels, J., Karduna, A.R., McQuade, K., Wang, X., Werner, F.W., Buchholz, B., 2005. ISB recommendation on definitions of joint coordinate systems of various joints for the reporting of human joint motion - Part II: Shoulder, elbow, wrist and hand. Journal of Biomechanics 38, 981–992.

[34] Yosibash, Z., Plitman Mayo, R., Dahan, G., Trabelsi, N., Amir, G., Milgrom, C., 2014. Predicting the stiffness and strength of human femurs with real metastatic tumors. Bone 69, 180–190.

[35] Yosibash, Z., Tal, D., Trabelsi, N., 2010. Predicting the yield of the proximal femur using high order finite element analysis with inhomogeneous orthotropic material properties. Phylosophical Transaction of the Royal Society: A 368, 2707–2723.

[36] Yosibash, Z., Trabelsi, N., Hellmich, C., 2008. Subject-Specific p-FE Analysis of the Proximal Femur Utilizing Micromechanics-Based Material Properties. International Journal for Multiscale Computational Engineering 6, 483–498.

Tables

Table 1: Mean strain, RMSE and mean error of FE and experiment data, arranged by bone's regions.

Bone region	Mean ABS strain [μs]	RMSE [μs] (%)	Mean ABS error [%]
Neck	850	242 (28.5)	19.8
Shaft	2859	484 (16.9)	18.9
All data	1936	392 (20.2)	18.3

Table 2: FFH3 & FFH4 yield & fracture loads summary according to both trabecular and cortical regions

Bone Label	Exp. Yield Load [N]	Exp. Ult. Load [N]	Predicted Yield Load by FEA [N]	
			Trabecular [2]	Cortical [15]
FFH3L	1300	1380	1040	1092
FFH3R	1280	1630	1248	1012
FFH4L	5000	5290	4160	4914
FFH4R	5000	5750	4160	4587

Table 3: Fracture location and classification for all fractured humeri

Humerus	Frature location and description	Classification	
		Neer	AO
FFH1R	Anatomical neck+GT (Varus)		C1.2
FFH1L	Anatomical neck+GT (Varus)		C1.2
FFH2R	Anatomical neck+GT (Valgus)		C1.1
FFH2L	Anatomical neck+GT (Valgus)	type	C1.1
FFH3R	Anatomical neck+GT (Varus)	II	C1.2
FFH3L	Anatomical neck		C1.3
FFH4R	Anatomical neck		C1.3
FFH4L	Anatomical neck		C1.3

Figures

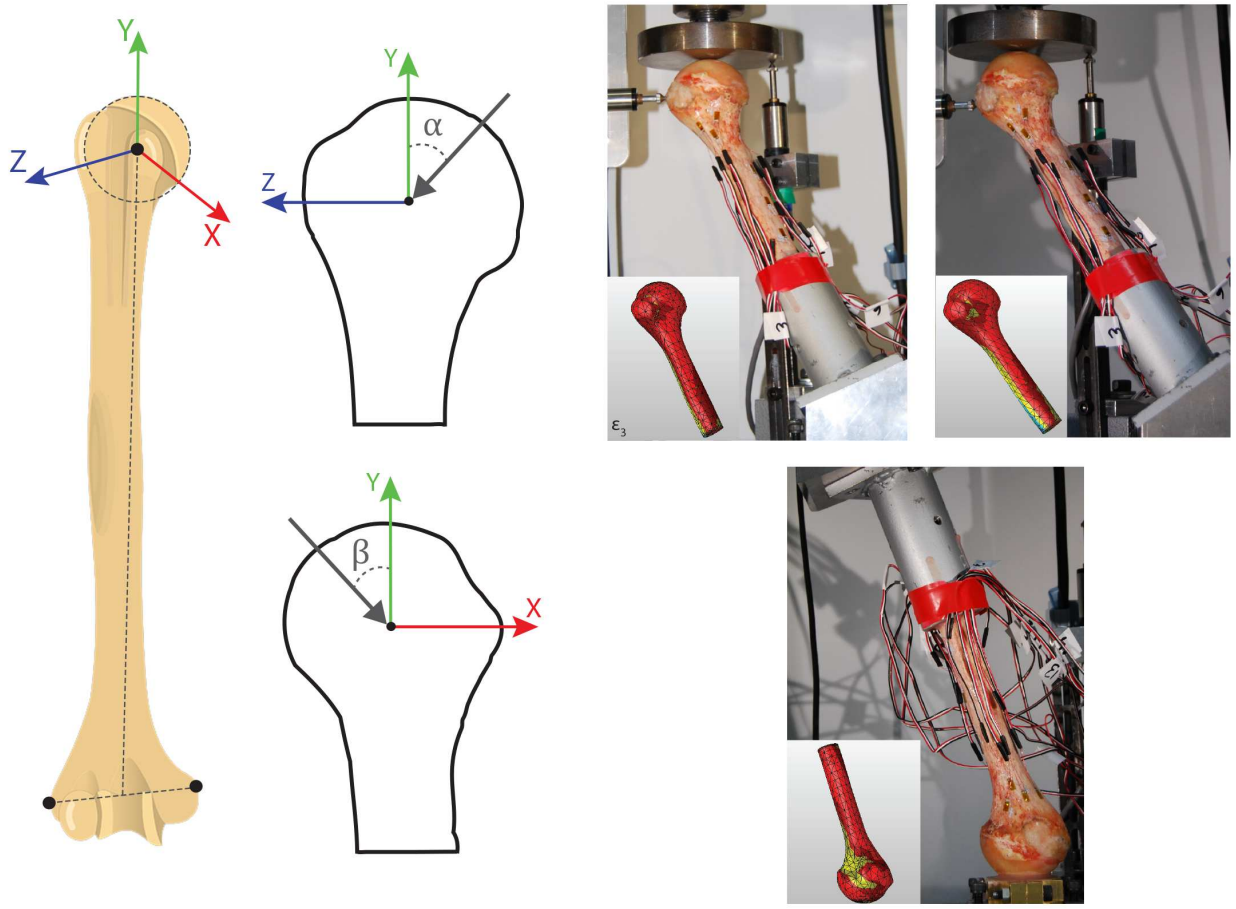

Figure 1: Left: Coordinate system of the proximal humerus and angles used to define loading vector. Right: Experiment loading configurations corresponding FEA showed on FFH4L.

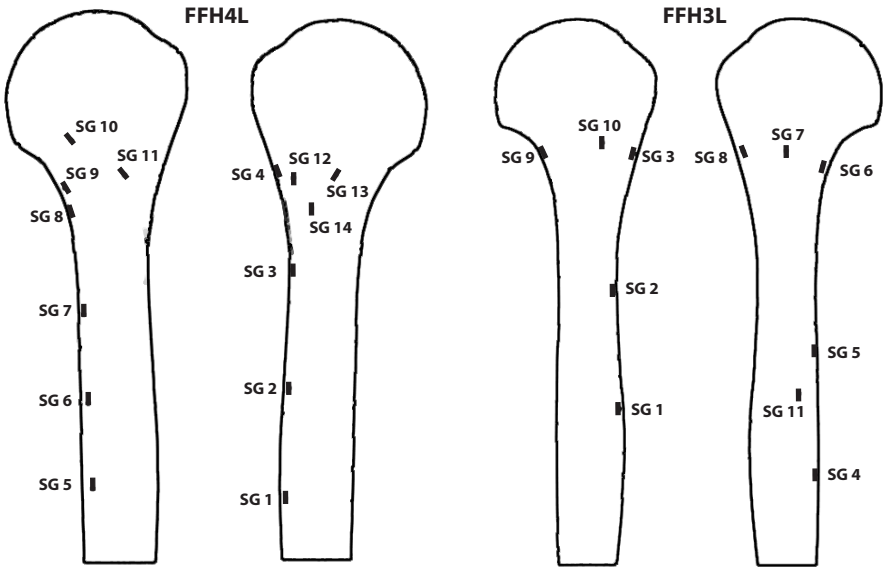

Figure 2: Strain gauge locations showed on left humeri. The locations are correspondingly located on the right bones.

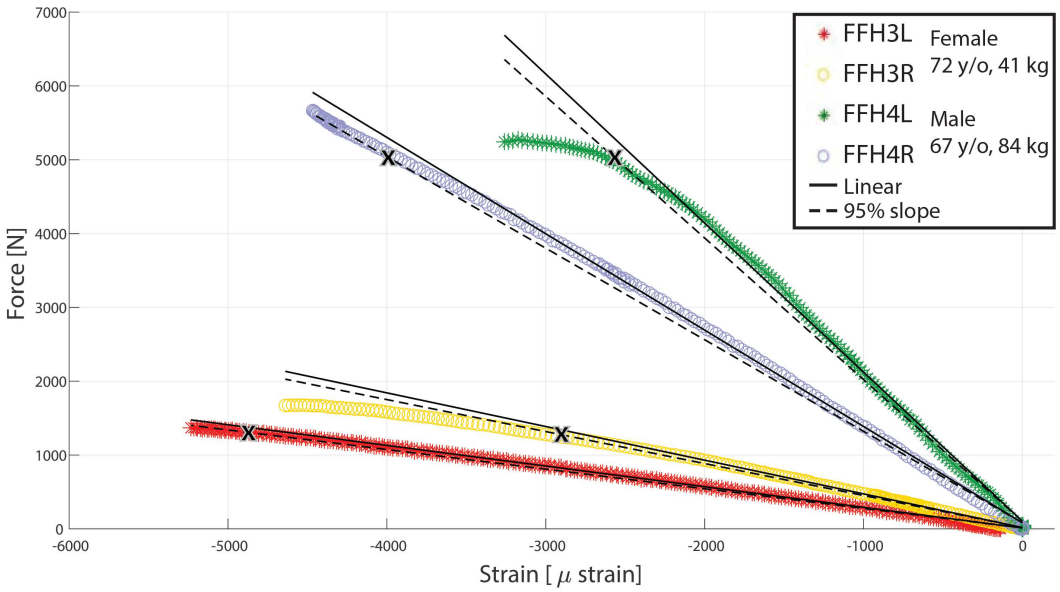

Figure 3: Force vs largest strains measured at the SG closest to the fracture location. Yield point was defined in the intersection of dashed line (95% of the linear slope) with the curve.

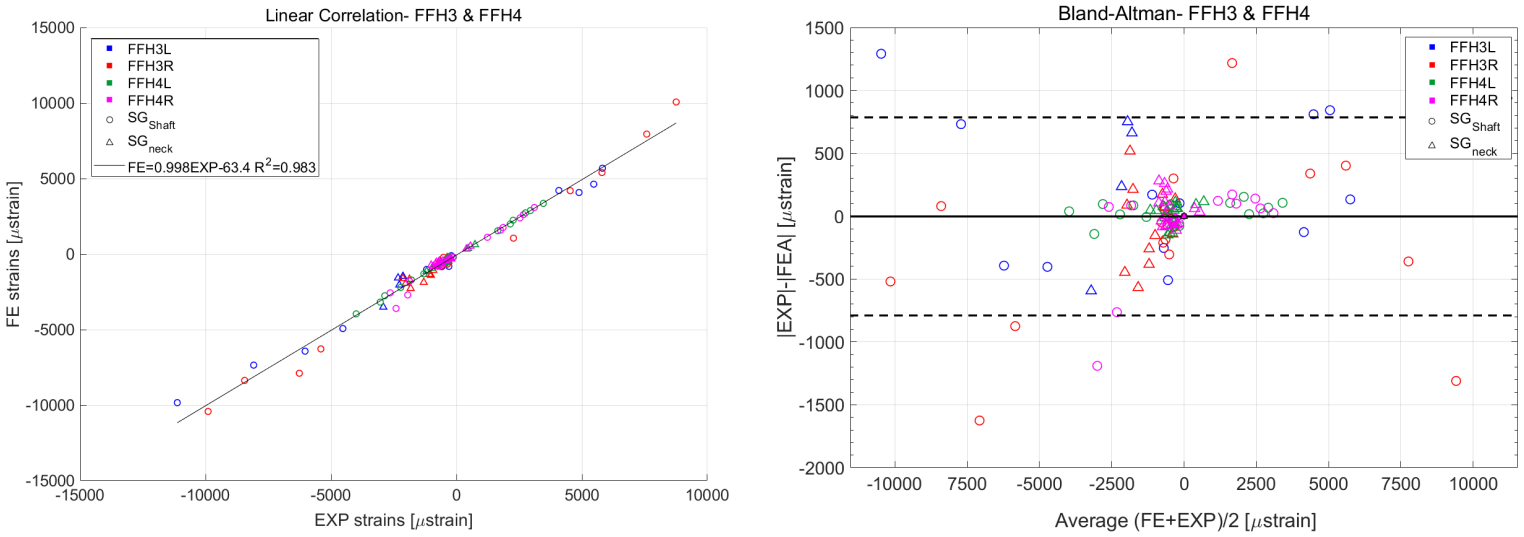

Figure 4: Linear correlation and Bland-Altman plots for FFH3 & FFH4. Different bones appear in different colors, circles and triangles refer to strain on bones' shaft and neck.

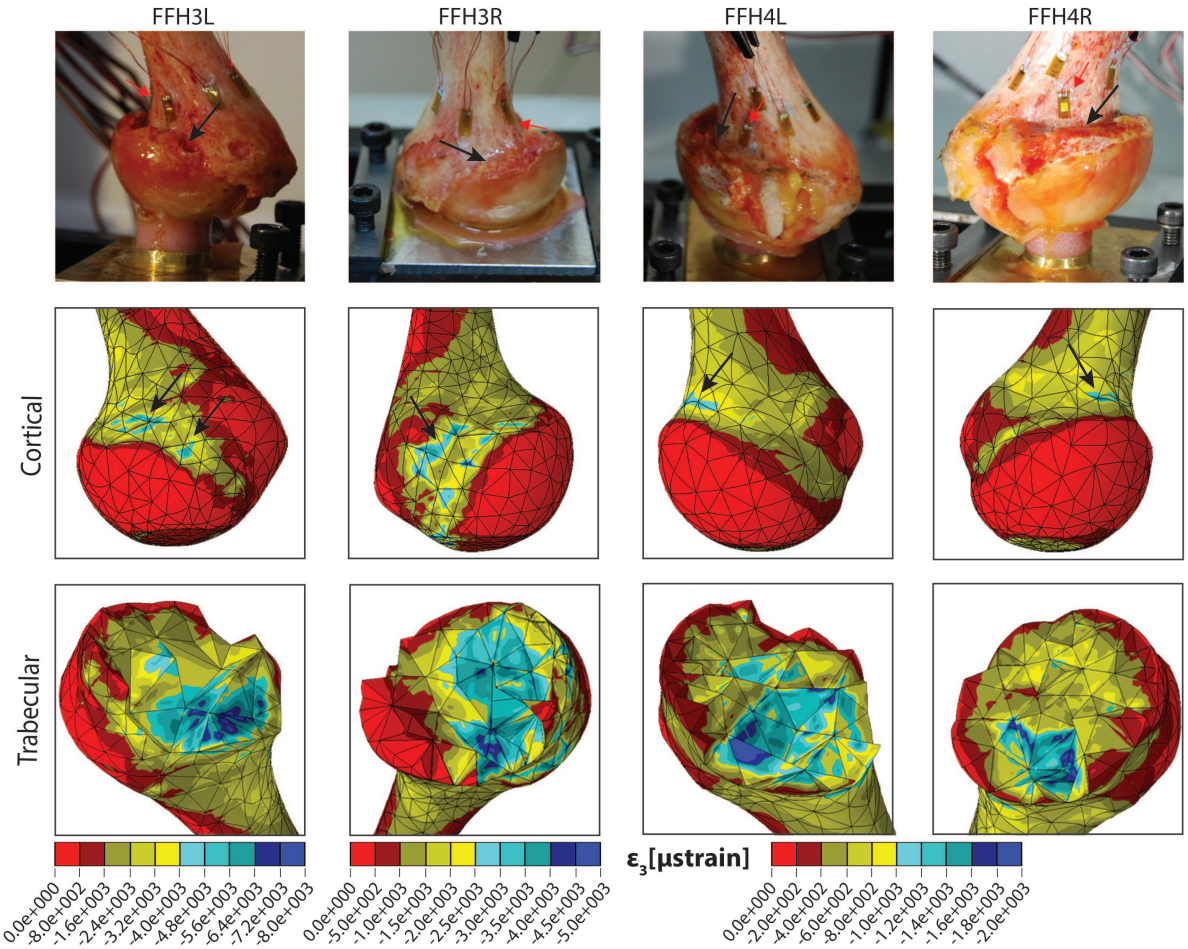

Figure 5: Fracture location and FEA max ε_3 strain ($\mu strain$) in both cortical and trabecular regions. Black arrows indicate fracture location/FE maximum strain, red arrows indicate the SG closest to fracture location

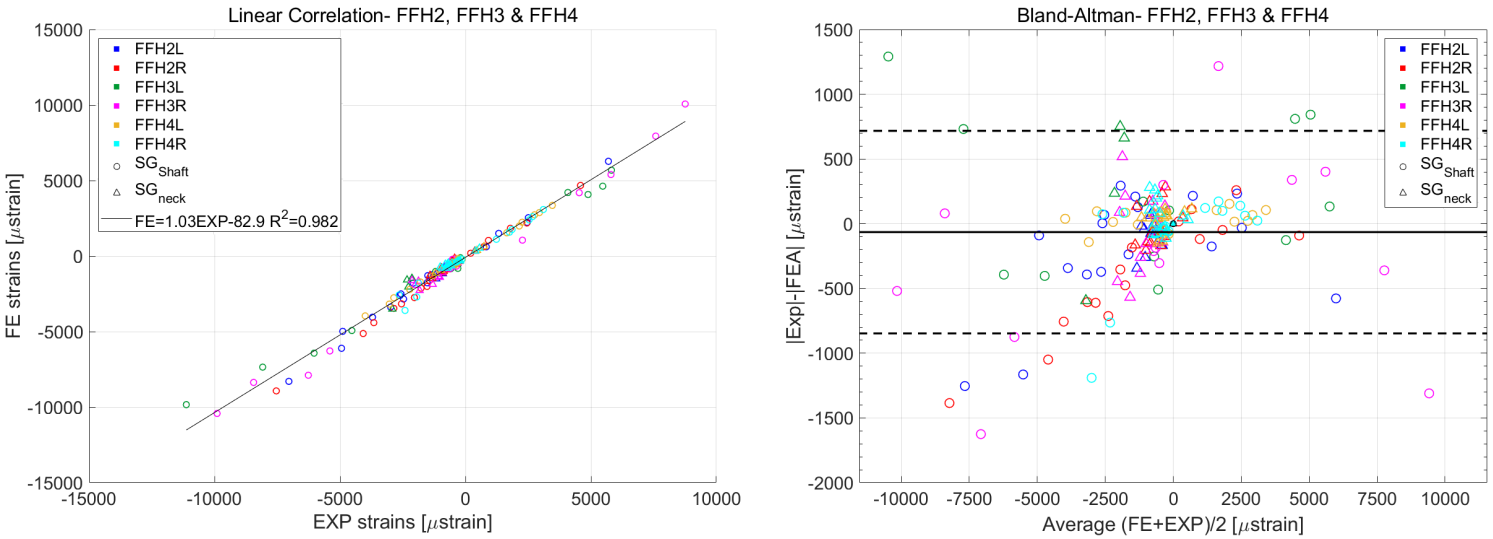

Figure 6: Linear correlation and Bland-Altman plots for FFH2, FFH3 & FFH4

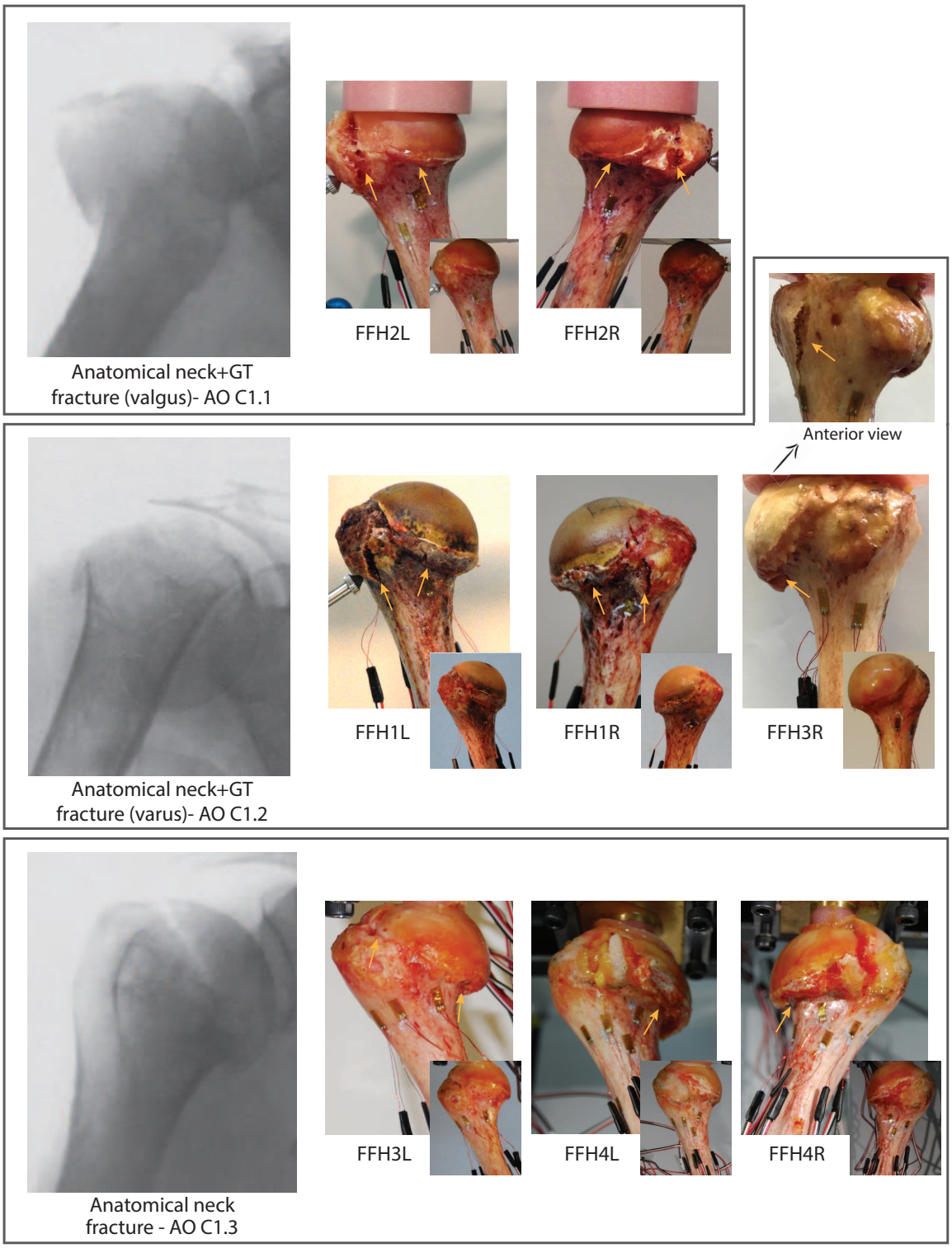

Figure 7: Fractured humeri arranged by their type according to the AO classification (smaller photos show the intact humeri). X-rays are taken from [24]. FFH1 & FFH2 experiments are from [9].